MIRO2 Regulates Prostate Cancer Cell Growth via GCN1-Dependent Stress Signaling

Madison Furnish[1,2], Dillon P. Boulton[1,2], Victoria Genther[1], Denisa Grofova[1], Mitchell Lee Ellinwood[1], Lina Romero[1], M. Scott Lucia[3], Scott D. Cramer[1], and M. Cecilia Caino[1]

ABSTRACT

There is a continued need to identify novel therapeutic targets to prevent the mortality associated with prostate cancer. In this context, mitochondrial Rho GTPase 2 (*MIRO2*) mRNA was upregulated in metastatic prostate cancer compared with localized tumors, and higher *MIRO2* levels were correlated with poor patient survival. Using human cell lines that represent androgen-independent or -sensitive prostate cancer, we showed that MIRO2 depletion impaired cell growth, colony formation, and tumor growth in mice. Network analysis of MIRO2′s binding partners identified metabolism and cellular responses to extracellular stimuli as top overrepresented pathways. The top hit on our screen, General Control Nonderepressible 1 (GCN1), was overexpressed in prostate cancer, and interacted with MIRO2 in prostate cancer cell lines and in primary prostate cancer cells. Functional analysis of MIRO2 mutations present in patients with prostate cancer led to the identification of MIRO2 159L, which increased GCN1 binding. Importantly, MIRO2 was necessary for efficient GCN1-mediated GCN2 kinase signaling and induction of the transcription factor activating transcription factor 4 (ATF4) levels. Further, MIRO2′s effect on regulating prostate cancer cell growth was mediated by ATF4. Finally, levels of activated GCN2 and ATF4 were correlated with MIRO2 expression in prostate cancer xenografts. Both MIRO2 and activated GCN2 levels were higher in hypoxic areas of prostate cancer xenografts. Overall, we propose that targeting the MIRO2-GCN1 axis may be a valuable strategy to halt prostate cancer growth.

Implications: MIRO2/GCN1/GCN2 constitute a novel mitochondrial signaling pathway that controls androgen-independent and androgen-sensitive prostate cancer cell growth.

Introduction

Patients diagnosed with metastatic prostate cancer face a 5-year survival rate of 30.2% [Surveillance Epidemiology and End Results (SEER) Program, NCI]. Hormone therapy targeting the androgen axis (therapeutic castration) is the mainstay therapy in prostate cancer (1). Because many tumors become resistant to castration but continue to be driven by androgen signaling, novel drugs that block androgen production or target the androgen receptor (AR) are used in the clinic (2–4). Unfortunately, resistance to second-generation AR-targeted therapies and progression to androgen-independent disease ultimately leads to prostate cancer–related death (3–7). For these patients, there are no effective treatments, highlighting the continued need to identify novel therapeutic targets to prevent the mortality associated with prostate cancer.

In this context, mitochondria play a central and multifunctional role in malignant tumor progression (8). In particular, mitochondrial signaling pathways have emerged as important nodes for tumorigenesis and metastatic dissemination (9–12). As a result, mitochondria-targeting strategies are being pursued in the clinic and there is a strong interest in identifying new mitochondrial pathways in cancer (8, 10). In this study, we focus on one novel mitochondrial pathway centered on mitochondrial Rho GTPase 2 [MIRO2; also known as Ras Homolog Family Member T2 (RHOT2)], a small GTPase of the Ras superfamily. In previous studies, we showed that *MIRO2* mRNA is upregulated in primary cancer *versus* normal tissues, across multiple tumor types (13). MIRO2 had been previously studied in the context of nontumorigenic cells, where it coordinates microtubule- and actin-based mitochondrial movement (14). However, we showed that cancer cells utilize MIRO2′s canonical function on mitochondrial trafficking exclusively under conditions of cellular stress that exacerbate mitochondrial dynamics (13, 15). In a recent study, Altieri and colleagues showed that Myc transcriptionally regulates *MIRO2*, which in turn modulates mitochondrial dynamics and tumor-cell invasion (16). Despite this evidence for a role of MIRO2 in cancer, we lack a comprehensive understanding of the function and regulation of MIRO2 in cancer cell biology.

The goals of this study were to examine the role of MIRO2 in driving tumor cell-intrinsic phenotypes in prostate cancer and to characterize the molecular pathway utilized by MIRO2 in this context. In prostate, *MIRO2* mRNA is upregulated in patients with recurred or progressed disease, and higher *MIRO2* levels correlate with poor patient survival. MIRO2 depletion in prostate cancer cell lines impaired cell growth, colony formation, and tumor growth in mice. Network analyses of MIRO2 coprecipitating proteins identified metabolism, cell cycle, and cellular responses to extracellular stimuli amongst the top overrepresented pathways. We characterized the role of the top hit on our screening, General Control Nonderepressible (GCN1) and found that GCN1 depletion mimicked MIRO2 depletion. Furthermore, MIRO2

[1]Department of Pharmacology, School of Medicine, University of Colorado Anshutz Medical Campus, Aurora, Colorado. [2]Pharmacology Graduate Program, University of Colorado Anshutz Medical Campus, Aurora, Colorado. [3]Department of Pathology, School of Medicine, University of Colorado Anshutz Medical Campus, Aurora, Colorado.

Note: Supplementary data for this article are available at Molecular Cancer Research Online (http://mcr.aacrjournals.org/).

Corresponding Author: M. Cecilia Caino, Department of Pharmacology, School of Medicine, University of ColoradoAnshutz Medical Campus, Research I North, 12800 East 19th Avenue, 6126, Aurora, CO 80045. Phone: 303-724-3528; E-mail: cecilia.caino@cuanschutz.edu

Mol Cancer Res 2022;20:607–21

doi: 10.1158/1541-7786.MCR-21-0374

controlled activation of GCN1 signaling *in vitro* and *in vivo*. Overall, we propose a new mechanism driving prostate cancer growth of both AR-independent and androgen-sensitive tumors.

Materials and Methods

Cell culture and cell lines

Human prostate adenocarcinoma (C4–2, ATCC, catalog no. CRL-3314, RRID:CVCL_4782; DU145, ATCC catalog no. HTB-81, RRID: CVCL_0105; and PC3, ATCC, catalog no. CRL-1435, RRID: CVCL_0035), glioblastoma (LN229, ATCC catalog no. CRL-2611, RRID:CVCL_0393), breast ductal carcinoma (BT549, ATCC, catalog no. HTB-122, RRID:CVCL_1092), and prostate epithelial cells [human primary epithelial cells (HPrEC); EP156T, ATCC, catalog no. CRL-3289, RRID:CVCL_RW45; RWPE1, ATCC, catalog no. CRL-11609, RRID:CVCL_3791) were obtained from ATCC, and maintained in culture according to the supplier's specifications. Parental and MIRO2 knockout (KO) near-haploid chronic myelogenous leukemia (HAP1) cells derived from the KBM-7 cell line (RRID: CVCL_A426) were obtained from Horizon Discovery Group (catalog no. HZGHC89941). Both wild-type (WT) and MIRO2 KO cell lines were sequenced to confirm the CRISPR/Cas9 editing of the MIRO2 allele, which had a 13-bp deletion in exon 6 that led to a stop codon at amino acid 51. Master stocks of cell lines were authenticated using short tandem repeat (STR) analysis (The University of Colorado Cancer Center Cell Culture Core, Aurora, CO) and tested for *Mycoplasma* with the ATCC Universal *Mycoplasma* Detection Kit (ATCC, #301012K). Cells were cultured for a maximum of 8 weeks (or 8 passages for prostate epithelial cells) and *Mycoplasma* testing was repeated upon freezing stable short hairpin RNA (shRNA) cell lines and prior to injecting in mice. Amino acid starved (AAS) Media contained 10% dialyzed FBS (Gemini Bio-Products, #100–108) in RPMI 1640 Media Medium w/o Amino Acids, Sodium Phosphate (US Biologicals, #R8999–04A) supplemented with 1 g of sodium bicarbonate.

Primary culture of human prostatic epithelial cells

Monolayer cultures of human prostatic epithelial cells were conducted as previously described (17) with minor modifications. Samples were obtained through an honest broker through the Pathology Shared Resource of the University of Colorado Cancer Center. The authors did not have access to patient identifiers and the Colorado Institutional Review Board considered the study exempt from human subject research. Briefly, areas of benign and tumor glands in a fresh prostatic cross section were identified by toluidine blue staining. Samples were obtained within one hour of surgical removal. The remaining areas where samples were removed were included in routine diagnostic blocks and hematoxylin and eosin (H&E) sections were used to assess glandular morphology and assign Gleason grades. Each patient sample was given a unique identifier (i.e., UCD1 or UCD2). Cultures grown from areas of greater than 90% tumor surrounding a location were designated cancer and were assigned constitutively activate (CA) to their name (i.e., UCD1-CA or UCD2-CA). Cultures grown from areas surrounded by 100% benign glands were designated benign and assigned B to their name (i.e., UCD1-B or UCD2-B). The fresh samples were processed exactly as described previously (17). Primary explants were grown on collagen-coated dishes in keratinocyte serum-free medium (KSFM) with supplements (Gibco). After primary outgrowth, the cells were frozen in aliquots for later use. Secondary cultures were grown on collagen-coated plates in MCDB105 (Gibco) plus supplements. All cultures were used at passage 2 or 3.

Antibodies and reagents

Antibodies to MIRO1 (Novus, catalog no. NBP1–89011, RRID: AB_11034143, diluted 1:1,000), MIRO2 (Thermo Fisher Scientific, catalog no. PA5–52960, RRID:AB_2646541, diluted 1:2,000), GCN1 (Abcam, catalog no. ab86139, RRID:AB_1925025, diluted 1:2,000), FLAG (clone M-2, Sigma-Aldrich, catalog no. F3165, RRID: AB_259529, diluted 1:5,000), Total GCN2 (Cell Signaling Technology, catalog no. 3302, RRID:AB_2277617, diluted 1:2,000), Phospho-GCN2 T899 (Abcam catalog no. ab75836, RRID:AB_1310260, diluted 1:1,000; Cell Signaling Technology, catalog no. 3301, RRID: AB_2095872, diluted 1:1,000), Phospho-eIF2α S51 (Cell Signaling Technology, catalog no. 3398, RRID:AB_2096481, diluted 1:1,000), Total-eIF2α (clone D7D3, Cell Signaling Technology, catalog no. 5324, RRID:AB_10692650, diluted 1:10,000), ATF4 (clone D4B8, Cell Signaling Technology, catalog no. 11815, RRID:AB_2616025, diluted 1:1,000), mTOR (clone#7C10, Cell Signaling Technology, catalog no. 2983, RRID:AB_2105622, diluted 1:1,000), DYN1HC1 (Proteintech, catalog no. 12345–1-AP, RRID:AB_2261765, diluted 1:5,000), MYO9B (Thermo Fisher Scientific, catalog no. PA5–18524, RRID: AB_10980408, diluted 1:250), PAXILLIN (clone 5H11, Thermo Fisher Scientific, catalog no. AHO0492, RRID:AB_2536312, diluted 1:1,000), BIG1 (Abcam, #ab72061, diluted 1:1,000), Vinculin (clone E1E9V, Cell Signaling Technology, catalog no. 13901, RRID: AB_2728768, diluted 1:400,000), and β-actin (clone AC-15, Sigma-Aldrich, catalog no. A5441, RRID:AB_476744, diluted 1:500,000) were used for Western blotting.

Animal studies

Size of experimental groups was calculated to detect a minimal difference of 40% between control and experimental groups, and 30% variability around the mean. Under these conditions, at 9 animals per group with expected effect size of 0.4 between the two compared groups at the two-sided 0.05 significance level, we have 80% power to detect differences. Experimenters were blinded until the end of the study, with one person preparing the cell suspensions, a second person assigning groups to letters, and a third person injecting animals and measuring tumors. Groups of 8-week-old outbred male immunocompromised athymic mice ($Foxn1^{nu}/Foxn1^{nu}$, The Jackson Laboratory, strain#007850 J:NU, RRID:IMSR_JAX:007850; 9 mice per group) were injected subcutaneously with either 1×10^6 PC3 cells or 2×10^6 DU145 cells stably transfected with control empty vector or two independent MIRO2-directed shRNA sequences (M2 a and b), and superficial tumor growth was quantified with a caliper. At the end of the experiment, animals were euthanized, and the xenografts were dissected and processed for IHC.

Statistics

Experiments were carried out in triplicates and data are expressed as mean ± SEM of multiple independent experiments (at least three independent experiments, $n = 3$). For descriptive data analysis, means, SD and medians were calculated, and distributions of data were examined to ascertain whether normal theory methods were appropriate. Student *t* test or Wilcoxon rank-sum test was used for two-group comparative analyses. For multiple-group comparisons, ANOVA or Kruskal–Wallis test with posthoc Bonferroni procedure were applied. Variance similarity between groups was tested with Fisher (two groups) or Bartlett (multiple groups) tests. All statistical analyses were performed using GraphPad Prism (RRID:SCR_002798) version 7.0 for Windows. A P value of <0.05 was considered as statistically significant.

Study approvals

Studies involving vertebrate animals (rodents) were carried out in accordance with the Guide for the Care and Use of Laboratory Animals (National Academies Press, 2011). The Institutional Animal Care and Use Committee (IACUC) of the University of Colorado (Aurora, CO) approved all animal experiments under Protocol #581. Studies using human primary prostate epithelial cells were considered exempt from human subject research by the Colorado Institutional Review Board.

Supplementary information Methods include detailed sections on plasmids, mutagenesis and transfections, gene silencing, Western blotting, endogenous coimmunoprecipitation (co-IP), FLAG IP, proteomics ID, mRNA quantitation, analyses of expression and cancer cell

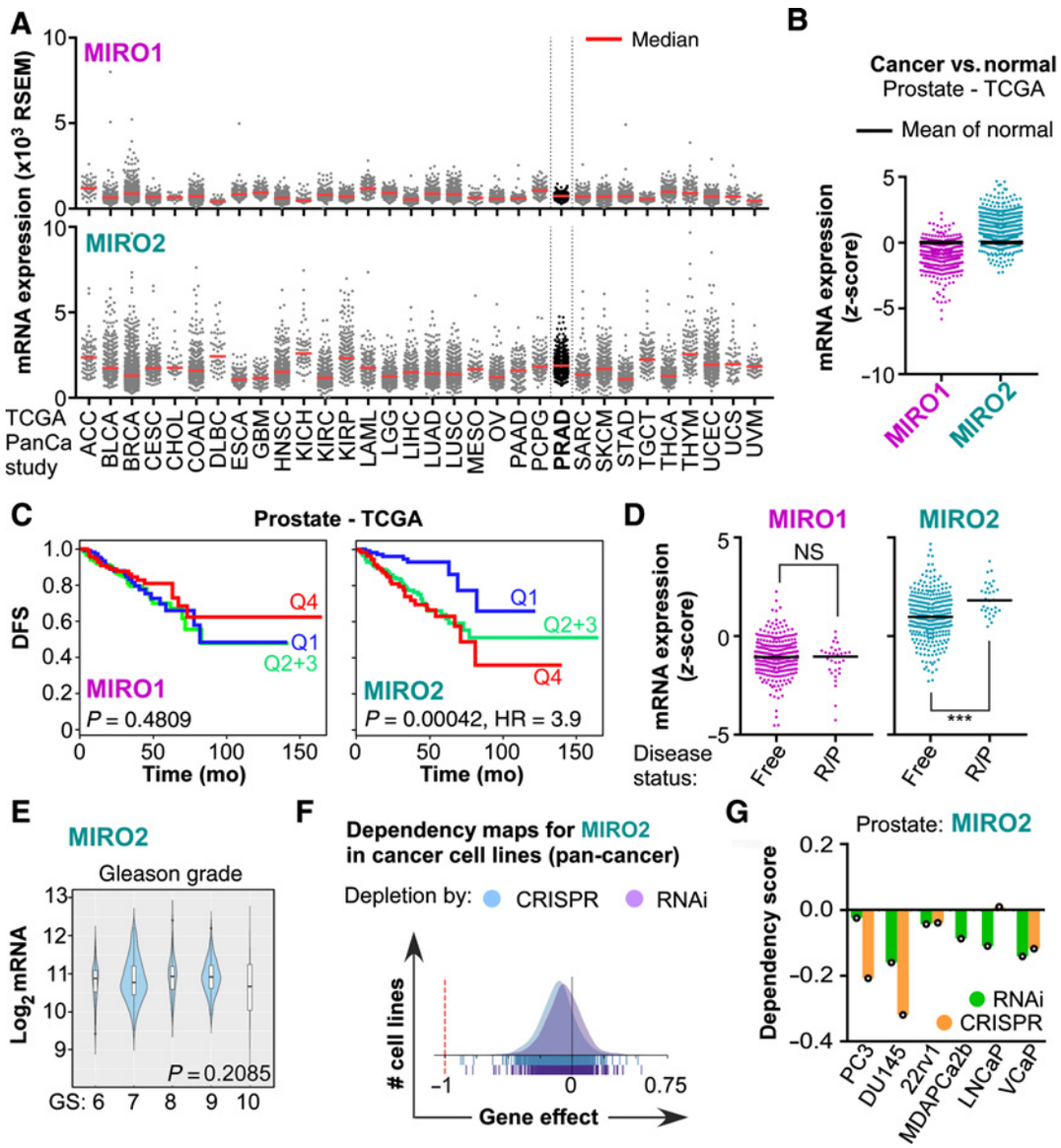

Figure 1.

MIRO1/2 alterations in cancer. **A,** The TCGA database was interrogated for *MIRO1/2* mRNA expression across tumor types. PanCA, PanCancer. **B,** Relative expression of *MIRO1/2* mRNA in cancer versus normal adjacent tissues on the prostate TCGA PanCancer study. **C,** Kaplan–Meier analyses based on *MIRO1/2* mRNA expression in human primary tumor samples. Datasets were split at quartiles (Q), where Q4>Q3>Q2>Q1. Q1 versus Q4 curves were compared with a Mantel–Cox test. HR was calculated with a Cox proportional hazards regression model. DFS, disease-free survival; mo, months. **D,** *MIRO1/2* expression according to disease free status. R/P, recurred/progressed. NS, not significant. ***, $P < 0.0001$ by *t* test with Welch correction. **E,** Violin plots depicting *MIRO2* expression among the Prostate TCGA dataset according to Gleason grade were generated using CANCERTOOL. GS, Gleason score. Groups were compared by ANOVA. **F,** The DepMap portal was searched for genetic cancer dependency on *MIRO2*. Gene effect scores are derived from DEMETER2 or CERES, with lower scores meaning a cell line is more likely to be dependent in the gene. A score of 0 represents nonessential genes, while -1 corresponds to the median of all common essential genes. **G,** Dependency scores in prostate cancer cell lines subject to RNAi or CRISPR-mediated depletion of MIRO2.

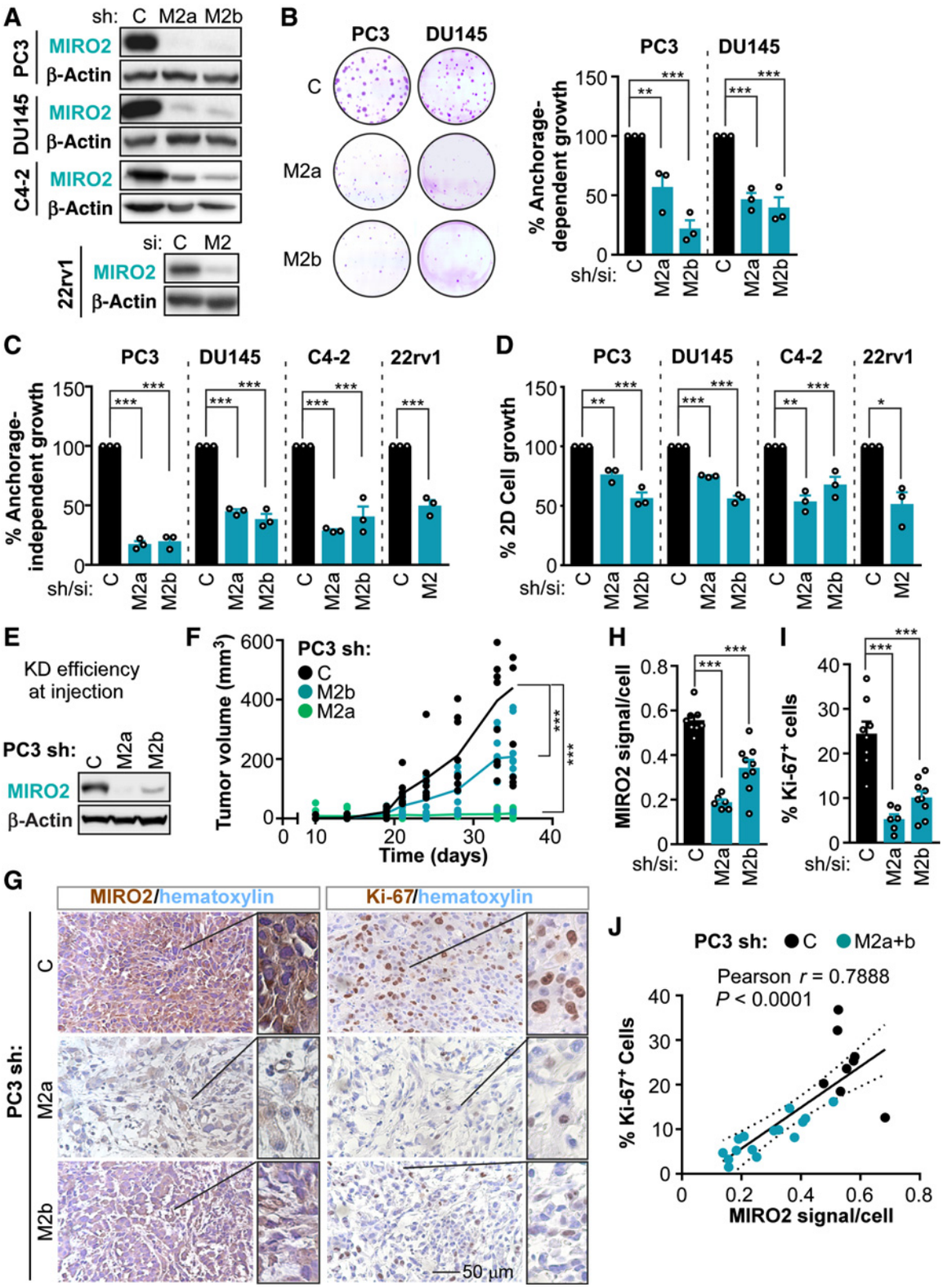
A
sh: C M2a M2b
PC3
MIRO2
β-Actin
DU145
MIRO2
β-Actin
C4-2
MIRO2
β-Actin
si: C M2
22rv1
MIRO2
β-Actin
B
PC3
DU145
C
M2a
M2b
PC3
DU145
% Anchorage-dependent growth
sh/si: C M2a M2b C M2a M2b
C
PC3
DU145
C4-2
22rv1
% Anchorage-independent growth
sh/si: C M2a M2b C M2a M2b C M2a M2b C M2
D
PC3
DU145
C4-2
22rv1
% 2D Cell growth
sh/si: C M2a M2b C M2a M2b C M2a M2b C M2
E
KD efficiency at injection
PC3 sh: C M2a M2b
MIRO2
β-Actin
F
PC3 sh:
C
M2b
M2a
Tumor volume (mm3)
Time (days)
H
MIRO2 signal/cell
sh/si: C M2a M2b
I
% Ki-67+ cells
sh/si: C M2a M2b
G
MIRO2/hematoxylin
Ki-67/hematoxylin
PC3 sh: C M2a M2b
50 μm
J
PC3 sh: C M2a+b
Pearson r = 0.7888
P < 0.0001
% Ki-67+ Cells
MIRO2 signal/cell

dependency from public databases, cell growth assays, proximity ligation assays, immunofluorescence and cortical mitochondria quantitation, and IHC.

Data availability statement

The mass spectrometry proteomics data have been deposited to the ProteomeXchange Consortium via the PRIDE (Pride-asap, RRID:SCR_012052) partner repository with the dataset identifier PXD029490 and 10.6019/PXD029490.

Results

MIRO2 alterations in prostate cancer

To examine the status of *MIRO2* in cancer, we searched the The Cancer Genome Atlas (TCGA) PanCancer Atlas database at cBioPortal (18, 19) for *MIRO2* expression, copy-number alterations, and mutations. We also investigated the status of the closely related *MIRO1*, as studies in nontumorigenic cells have shown functional redundancy between MIRO1 and MIRO2 (14, 20, 21). We found that *MIRO2* mRNA is expressed at variable levels across tumor types, with prostate adenocarcinoma showing one of the highest medians (**Fig. 1A**). Interestingly, *MIRO2* is expressed at higher levels than *MIRO1* in the same tumor types (**Fig. 1A**). In the TCGA prostate adenocarcinoma cohort, *MIRO1* and *MIRO2* expression are oppositely regulated in cancer versus normal adjacent tissue (**Fig. 1B**). Likewise, higher *MIRO2* expression in prostate cancer compared with normal prostate was observed in other patient cohorts, including the Grasso and Lapointe datasets (Supplementary Fig. S1A). Furthermore, higher *MIRO2* expression is correlated with poor patient survival in the TCGA cohort, while there is no correlation with *MIRO1* expression in the same patient cohort (**Fig. 1C**). A second patient cohort showed a trend for higher levels of *MIRO2* association with poor patient survival (Supplementary Fig. S1D). Recurred or progressive disease, as well as metastatic disease, were associated with higher *MIRO2* expression as well (**Fig. 1D**; Supplementary Fig. S1B). On the other hand, there is no relationship between expression of *MIRO2* and Gleason grade of the tumors (**Fig. 1E**; Supplementary Fig. S1C). At the genomic level, *MIRO2* is commonly altered in prostate, breast, and pancreas tumors (Supplementary Fig. S1E). Mutations in *MIRO2* are randomly distributed, with a small number of more frequent sites associated with functional domains (Supplementary Fig. S1F). Overall, *MIRO2* is expressed across disparate tumor types and upregulation in prostate cancer was associated with poor prognosis and metastatic disease.

As a first way to examine genetic dependency of cancer cells on *MIRO2*, we turned to the Cancer Dependency Map project from the Broad Institute (Cambridge, MA). Depletion of *MIRO2* in a large panel of pan-cancer cell lines by RNA inhibition (RNAi) or CRISPR/Cas9 gene editing reduced cancer cell growth in the majority of cell lines tested (**Fig. 1F**). In a panel of prostate cancer cell lines, *MIRO2* depletion reduced cell growth (score < 0) in all cell lines tested (**Fig. 1G**). In summary, *MIRO2* is overexpressed in prostate cancer and prostate cancer cells are uniformly dependent in *MIRO2* for cell growth.

MIRO2 controls prostate cancer cell growth

In prostate cancer cell lines that do not express AR (PC3 and DU145), MIRO2 depletion impaired anchorage-dependent (Fig. 2A and B), anchorage-independent (**Fig. 2C**), and **2D** cell growth (**Fig. 2D**). Furthermore, anchorage-independent growth and **2D** cell growth were impaired in the androgen-sensitive cell lines (22, 23) C4–2 and 22rv1 (**Fig. 2C** and **D**). In contrast, MIRO1 depletion had no effect on anchorage-dependent growth (Supplementary Fig. S2A and S2B) or **2D** cell growth (Supplementary Fig. S2C and S2D), indicating nonredundant roles for MIRO1 and MIRO2 in prostate cancer cell biology.

Next, we evaluated the kinetics of tumor growth *in vivo*. We found that MIRO2 depletion impaired tumor growth in mice in two separate AR-independent xenograft models (PC3, **Fig. 2E** and **F**; and DU145, Supplementary Fig. S2E–S2G). Of note, the majority of the DU145 xenograft tumors lost the stable KD of MIRO2 by the end of the experiment (Supplementary Fig. S2F). When grouping the animals based on whether MIRO2 remained KD at the endpoint, the effects on inhibition of tumor growth on DU145 xenografts were quite similar to the ones observed in PC3 xenografts (Supplementary Fig. S2G, right panels). Taken together, higher efficiency of MIRO2 depletion led to stronger effects on tumor growth inhibition. Furthermore, the proliferative index of MIRO2-depleted tumors was significantly lower compared with control (PC3, **Fig. 2G–I**; and DU145, Supplementary Fig. S2I–S2H). Higher MIRO2 levels strongly correlated with higher proliferation in xenografts (**Fig. 2J**; Supplementary Fig. S2K). In sum, MIRO2 controls several tumor cell-intrinsic phenotypes that support prostate cancer cell growth *in vitro* and *in vivo*.

Novel effectors of MIRO2 in prostate cancer

A key question stemming from our studies was what are the mechanisms by which MIRO2 supports tumor cell growth in prostate cancer? As MIRO2 has been linked to mitochondrial subcellular localization at the cortical cytoskeleton in response to therapy and oncogene-induced stress (13, 15, 16), we first analyzed the distribution of mitochondria in control and MIRO2-depleted cells growing in normal conditions (e.g., nonstressed). Using a

Figure 2.

MIRO2 depletion impairs tumor cell intrinsic phenotypes. Stable knockdown of MIRO2 was achieved by shRNA in PC3, DU145, and C4–2 cells; or by siRNA in 22rv1 cells. **A,** control sh/si; M2a/b, MIRO2-targeting shRNAs (two independent sequences, a and b); M2 (MIRO2-targeting siRNA pool). **B,** Representative blots showing the efficiency of knockdown; and anchorage-dependent growth at 14 days postplating. Left, Representative scans of stained colonies. Right, quantitation of colony number per well, relative to control and represented as mean ± SEM ($n = 3$). *, $P = 0.0112$; ***, $P < 0.001$ by one-way ANOVA and Dunnett posttest for multiple comparisons. C, control. **C,** Anchorage-independent growth in soft agar at 14 days postplating. Colony number per well relative to control is represented as mean ± SEM ($n = 3$). ***, $P < 0.001$ by one-way ANOVA and Dunnett posttest for multiple comparisons; or test for pairwise comparisons on 22rv1. C, control. **D,** 2D cell growth at 72 hours postplating was determined by a MT-Glo assay and relativized to the control. Data is represented as mean ± SEM ($n = 3$). *, $P < 0.05$; **, $P < 0.01$; ***, $P < 0.001$ by one-way ANOVA and Dunnett posttest for multiple comparisons; or *t* test for pairwise comparisons on 22rv1. C, control. **E** to **J**, Cells were injected subcutaneously into the flanks of male nude mice and tumor growth was followed by caliper measurements. **E,** Immediately after injection, cells were pelleted and analyzed for efficiency of knockdown by Western blot. **F,** Data are represented as individual tumors with the line connecting the mean of each group ($n = 9$ for control or M2b; $n = 6$ for M2a). Only 6 of 9 injected animals developed tumor in the M2a group. ***, $P < 0.001$ by two-way ANOVA. **G,** Tumors from (**F**) were processed for IHC at the endpoint of the experiment and assayed for MIRO2 levels or proliferation by staining with Ki-67 antibody and hematoxylin. A representative field (magnification 40X) is shown. **H** and **I,** Data are represented as mean ± SEM ($n = 9$ for control or M2b; $n = 6$ for M2a). ***, $P < 0.001$ by one-way ANOVA and Dunnett posttest for multiple comparisons. **J,** Correlation between percentage of Ki-67$^+$ cells and MIRO2 signal/cell in tumors from (**G**).

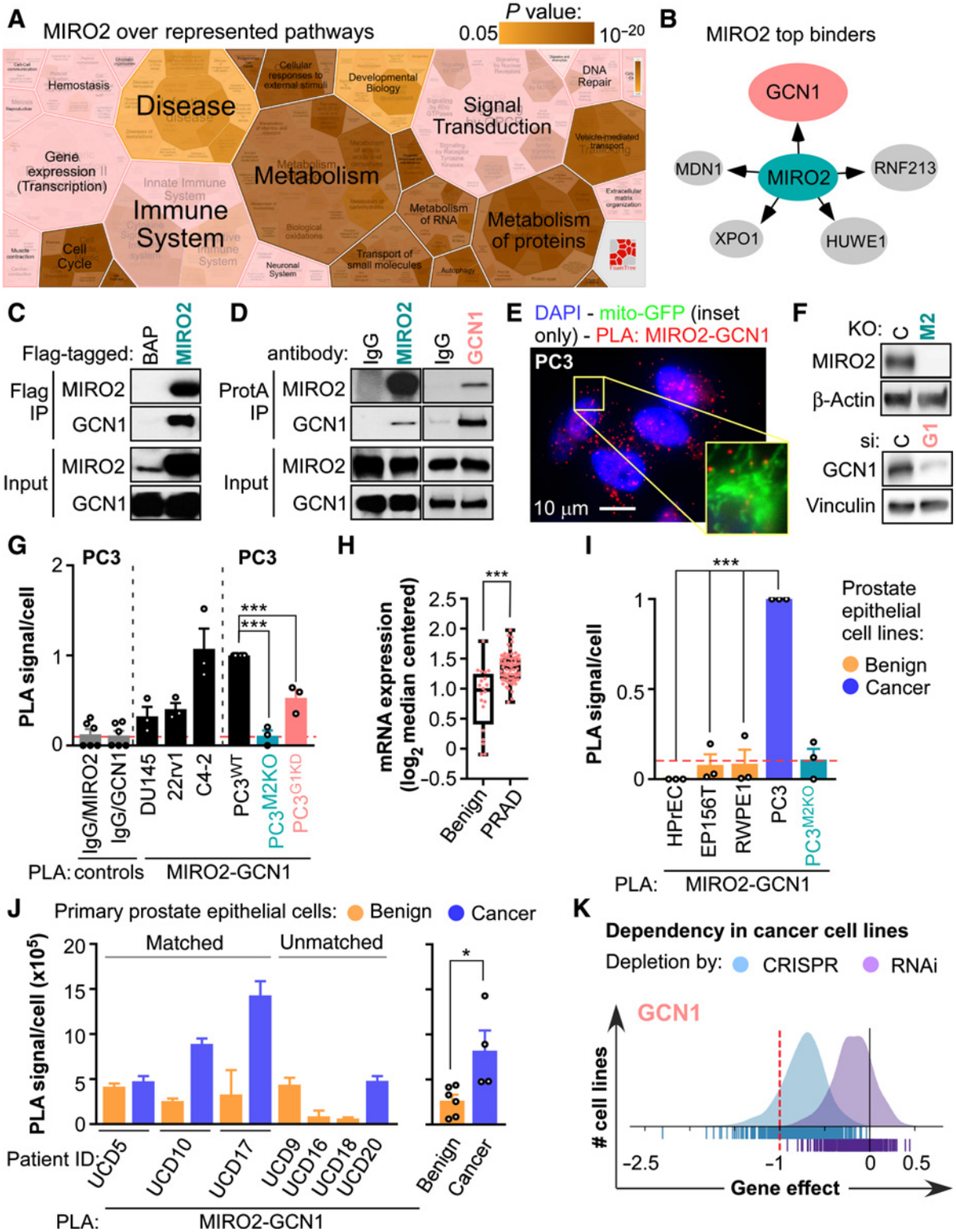

Figure 3.

Identification of novel effectors of MIRO2 in prostate cancer. **A,** MIRO2-Flag was immunoprecipitated from PC3 cells and protein binders were tryptically digested and identified by shotgun proteomics. A BAP-Flag was immunoprecipitated and subjected to proteomics analysis as a negative control. The Reactome FoamTree shows the overrepresented functional pathways identified by proteomics ID of MIRO2-IP. **B,** Top five MIRO2 binders identified in the proteomics screen, according to spectral counts. **C,** PC3 cells transiently expressing BAP-Flag or MIRO2-Flag were subject to Flag-IP and analyzed by Western blotting for co-IP of GCN1. A representative blot from $n = 3$ experiments is shown. (*Continued on the following page.*)

panel of prostate cancer, glioblastoma, breast, and leukemia cells, we found no differences in cortical mitochondrial localization between control and MIRO2-depleted cells (Supplementary Fig. S3A and S3B). Thus, cell growth defects are not associated with alterations in MIRO2-dependent mitochondrial localization under normal growth conditions.

Recent studies in nontumorigenic cells suggest that MIRO2 might have overlapping functions with MIRO1 in regulating mito-ER contacts, mitophagy, and mitochondrial shape (14, 21, 24–26). As contextual signals for neurons, hepatocytes, or fibroblasts likely do not overlap with those for epithelial cancer cells, we decided to take an unbiased approach to learn the molecular function of MIRO2 in cancer. MIRO2 is a member of the Ras superfamily of small GTPases (27). Small GTPases are molecular switches that bind effectors, which in turn activate signaling cascades and gene expression programs (28–30). Thus, we reasoned that identifying MIRO2′s protein binding partners would shed light on the molecular function of MIRO2 in prostate cancer.

To this end, we identified the proteins coprecipitating with FLAG-MIRO2 from PC3 cells (Supplementary Tables S1 and S2). Network analysis of MIRO2 binding partners identified metabolism, cell cycle, and cellular responses to extracellular stimuli amongst the top over-represented pathways (**Fig. 3A**; Supplementary Table S3). The top 50 coIP protein candidates based on spectral counts are presented in Supplementary Table S1. These include metabolism-related enzymes, protein kinases, and protein kinase regulators (GCN1, mTOR, SYFA, TECR, CMC1, SFXN3, QCR2, NDUS1, CMC2, FADS2, SQOR, ACSL3, M2OM); ubiquitin ligases/deubiquitinases and proteasome-related proteins (RN213, HUWE1, UBR4, USP9X, ECM29, BIRC6, FAF2); chaperones and cochaperones (BAG6, MDN1, DNJA1); organelle structure, posttranslational modification and trafficking proteins (BIG1, RPN2, MON2, EHD4, GET4, EHD1); and organelle import/export proteins (XPO1, XPO2, NU205, IPO5, IPO7). We validated candidate proteins ranging in spectral counts between 20 to 200 in FLAG-MIRO2 co-IP and found that six of six were confirmed to co-IP with FLAG-MIRO2 using endogenous antibodies for the protein candidates (Supplementary Fig. S3C).

We decided to follow up the top hit on the screen, GCN1 (**Fig. 3B** and **C**). Interestingly, GCN1 was included in both metabolism and cellular responses to extracellular stimuli pathways. In reciprocal co-IPs, GCN1 was bound to endogenous MIRO2 (**Fig. 3D**). The MIRO2-GCN1 interaction was detected by proximity ligations assays (PLA) in all prostate cancer cells models tested (**Fig. 3E–G**; Supplementary Fig. S3D). As expected based on MIRO2 anchoring to the mitochondrial outer membrane, most of the PLA signal overlaid with mitochondrially targeted GFP (**Fig. 3E**, inset). Because both *MIRO2* and *GCN1* mRNA have higher expression in prostate cancer than normal adjacent prostate tissues (**Fig. 1B** and **Fig. 3H**), we compared the levels of MIRO2-GCN1 interaction across benign and cancer cell lines. We observed that the MIRO2-GCN1 interaction was nearly undetectable by PLA in diploid and immortalized benign prostate epithelial cells, compared with prostate cancer cell lines, which showed strong interaction (**Fig. 3I**; Supplementary Fig. S3D). However, benign and cancer cell lines expressed equal levels of MIRO2 and GCN1 (Supplementary Fig. S3F), suggesting that the differential PLA signal is not explained by changes in expression of either protein. Furthermore, expression of IMPACT, an endogenous inhibitor of GCN1-GCN2 binding (29), was equal between benign and cancer cell lines (Supplementary Fig. S3F). Next, we wanted to show clinical relevance of this pathway using matched primary prostate epithelial cells isolated from patients. We found that the MIRO2-GCN1 interaction was much higher in primary prostate epithelial cancerous cells compared with benign cells (**Fig. 3J**; Supplementary Fig. S3E). Overall, MIRO2-GCN1 robustly interact in prostate cancer cell lines and primary prostate cancer cells, but the interaction is undetectable in benign cell lines and benign primary cells.

GCN1 is the upstream activator of GCN2/EIF2AK4, a serine/threonine kinase that senses amino acid availability, redox status, and actin dynamics cues in cells (29, 30). A recent study linked GCN1 to cell cycle regulation and proliferation in developing mice (31). However, there is no evidence of GCN1′s importance for cancer cells. Thus, as a first way to examine the role of GCN1 in controlling tumor cell growth, we mined the Cancer Dependency Map. Similar to MIRO2 (**Fig. 1F**), depletion of GCN1 in a large panel of pan-cancer cell lines by RNAi or CRISPR/Cas9 gene editing reduced cancer cell growth in most cell lines tested (**Fig. 3K**). As GCN1 ranked in the topmost dependent genes in more than 90% of the cell lines, GCN1 is considered a common essential gene in cancer. Thus, GCN1 is upregulated in prostate cancer, is a critical pan-cancer mediator of cell growth and is a novel binding partner for MIRO2.

GCN1 and GCN2 regulate prostate cancer cell growth

The importance of GCN2 was recently underscored by activation of GCN2 signaling in human breast, lung, and liver tumors (32). Furthermore, GCN2 is essential for leukemia, melanoma, and fibrosarcoma xenograft growth in mice (32–34). Interestingly, recent studies have linked mitochondrial stress to the activation of GCN2 and retrograde signaling to the nucleus in worms and mammalian cells (35, 36). Altogether, we postulate that GCN1 and GCN2 are key mediators of MIRO2′s effect on tumor cell growth in prostate cancer.

In order to determine if GCN1 and GCN2 control prostate cancer cell growth, we focused on a panel of prostate cancer cell lines from the Cancer Dependency Map. Similar to MIRO2 (**Fig. 1G**), GCN1 depletion via RNAi or CRISPR/Cas9 gene editing reduced cell growth (score < 0) in all cell lines tested (**Fig. 4A**). GCN2 depletion impaired cell growth as well, albeit to a lesser extent (**Fig. 4A**). To corroborate the results of the Cancer Dependency Map screen, we next depleted MIRO2 in AR-independent and androgen-sensitive prostate cancer cell lines (**Fig. 4B**). We found that stable GCN1 or GCN2 depletion reduced anchorage-dependent growth

(*Continued.*) **D,** Endogenous MIRO2 or GCN1 were immunoprecipitated from PC3 cells, and analyzed for co-IP of GCN1 or MIRO2, respectively. IgG was used as an isotype control. A representative blot from $n = 3$ experiments is shown. **E,** PLA assays to detect MIRO2/GCN1 proteins proximity in PC3 cells. A representative image (magnification 60X) is shown. Inset shows overlay between mitochondrially-targeted GFP and the PLA signal. **F,** Western blotting of PC3 cells bearing MIRO2 (M2) or GCN1 (G1) knockdown. **G,** PLA assays to detect MIRO2/GCN1 proteins proximity in PC3 cells. PLA using IgG and MIRO2 antibodies were used as negative controls. Specificity of the PLA was assayed by removing either MIRO2 (M2) or GCN1 (G1) and probing for the MIRO2/GCN1 interaction. PLA intensity per cell was represented as mean ± SEM ($n = 3$). ***, $P < 0.001$ by ANOVA and Dunnett posttest for multiple comparisons. **H,** GCN1 mRNA expression in benign prostate gland ($n = 20$) or prostate adenocarcinoma ($n = 69$) in the Wallace dataset. ***, $P = 0.0004$ by t test with Welch correction. **I** and **J,** PLA assays to detect MIRO2/GCN1 proteins proximity in the indicated benign or cancer primary prostate epithelial cells. Left, PLA intensity per cell was represented as mean ± SD ($n = 9$–14 independent fields). Right, data are represented as mean ± SEM ($n = 3$–5). *, $P = 0.0224$ by unpaired t test. **K,** The DepMap portal was searched for genetic cancer dependency on GCN1. Gene effect scores are derived from DEMETER2 or CERES.

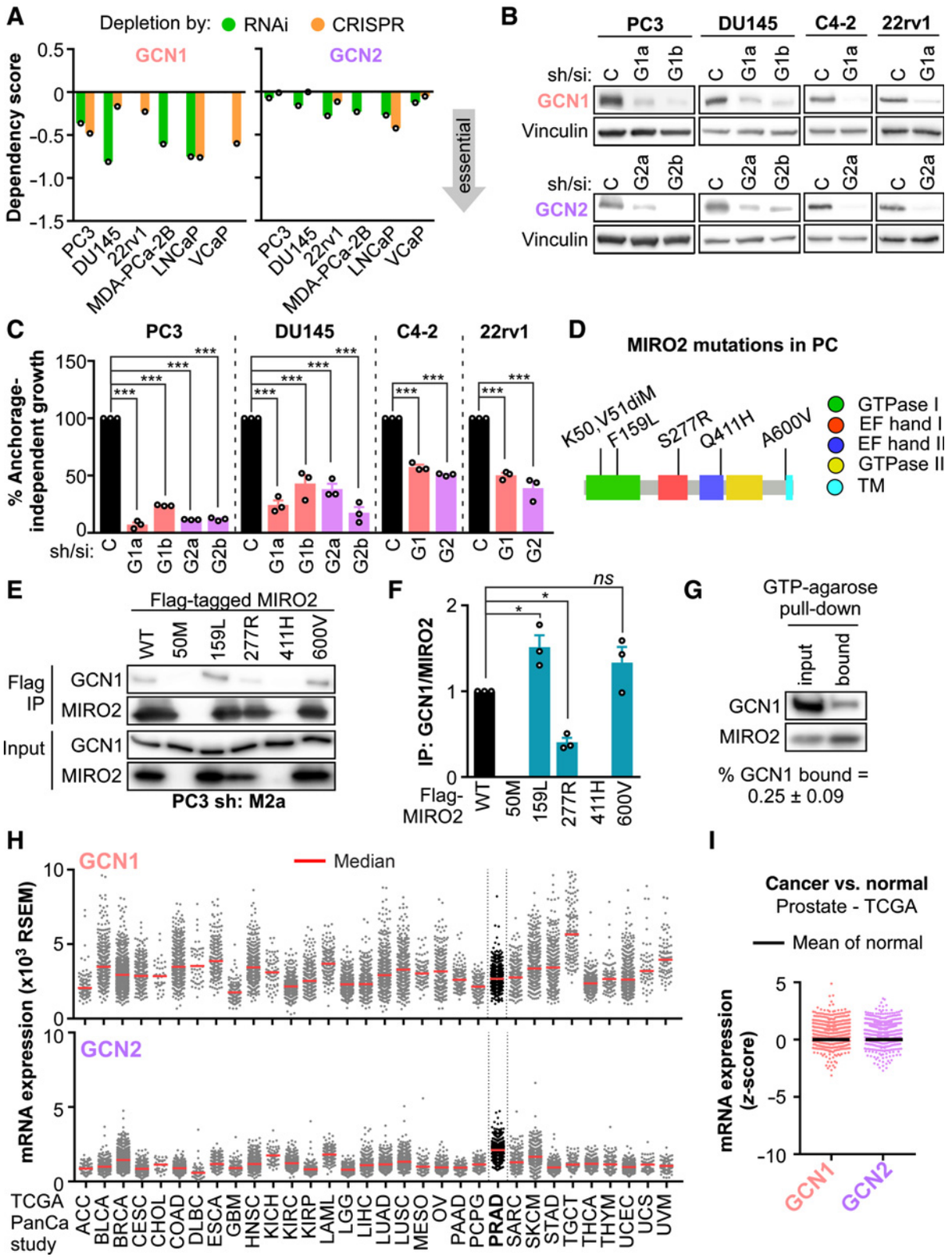
A
Depletion by: RNAi CRISPR
GCN1
GCN2
Dependency score
0.5
0
-0.5
-1.0
-1.5
PC3
DU145
22rv1
MDA-PCa-2B
LNCaP
VCaP
essential
B
PC3
DU145
C4-2
22rv1
sh/si: C G1a G1b
GCN1
Vinculin
sh/si: C G2a G2b
GCN2
Vinculin
C
PC3
DU145
C4-2
22rv1
% Anchorage-independent growth
150
100
50
0
***
sh/si: C G1a G1b G2a G2b
C G1 G2
D
MIRO2 mutations in PC
K50,V51diM
F159L
S277R
Q411H
A600V
GTPase I
EF hand I
EF hand II
GTPase II
TM
E
Flag-tagged MIRO2
WT 50M 159L 277R 411H 600V
Flag IP
GCN1
MIRO2
Input
GCN1
MIRO2
PC3 sh: M2a
F
IP: GCN1/MIRO2
2
1
0
ns
*
Flag-MIRO2
WT 50M 159L 277R 411H 600V
G
GTP-agarose pull-down
input
bound
GCN1
MIRO2
% GCN1 bound = 0.25 ± 0.09
H
GCN1
Median
mRNA expression (x10³ RSEM)
10
5
0
GCN2
TCGA PanCa study
ACC BLCA BRCA CESC CHOL COAD DLBC ESCA GBM HNSC KICH KIRC KIRP LAML LGG LIHC LUAD LUSC MESO OV PAAD PCPG PRAD SARC SKCM STAD TGCT THCA THYM UCEC UCS UVM
I
Cancer vs. normal
Prostate - TCGA
Mean of normal
mRNA expression (z-score)
5
0
-5
-10
GCN1
GCN2

(Supplementary Fig. S4A and S4B) and anchorage-independent cell growth (**Fig. 4C**). Thus, we established that GCN1 and GCN2 are critical mediators of prostate cancer growth.

In order to gain more insight into the regulation of the MIRO2-GCN1 interaction in prostate cancer, we turned to the prostate cancer patient cohorts available via cBioPortal. We identified six mutations distributed throughout the different domains of MIRO2 (**Fig. 4D**) and generated these site-directed mutants for functional analysis. Two mutant proteins were not detectable in whole cell lysates (50M and 411H), with the other four being expressed at similar levels (**Fig. 4F**). In FLAG-IP experiments, we identified one MIRO2 mutation that increased (F159L), and one that decreased (S277R), MIRO2-GCN1 binding (**Fig. 4E** and **F**). Because the location of the 159 L is within the *N*-terminal GTPase domain, and contradictory evidence on whether GTPase activity is important in the context of modulating MIRO2′s functions in nontumorigenic cells, we decided to investigate whether the GTPase activity of MIRO2 is required for binding to GCN1. First, we pulled down MIRO2 with nonhydrolysable GTP conjugated beads, and found GCN1 present on the pull-down fraction (**Fig. 4G**; approximately 0.25% of GCN1 was bound to GTP-MIRO2). Next, we generated point mutations of MIRO2 in either the *N*-terminal or *C*-terminal GTPase domains reported to CA or act as dominant negative (DN; refs. 14, 20, 21). Furthermore, we generated double mutants of MIRO2 where the *N*- and *C*-terminal GTPases were present in all possible combinations (Supplementary Fig. S4B). We expressed these FLAG-tagged MIRO2 mutants in PC3 cells bearing MIRO2 KD, and by FLAG-IP we found that all mutants bound similar amounts of GCN1 (Supplementary Fig. S4B and S4C), ruling out a potential contribution of the GTPase activity of MIRO2 for binding to GCN1.

Next, we interrogated the TCGA PanCancer Atlas database at cBioPortal (18, 19) for expression of *GCN1* and *GCN2* in cancer. We found that *GCN1* and *GCN2* mRNA are expressed at variable levels across tumor types, with prostate adenocarcinoma showing one of the highest medians (**Fig. 4H**). Furthermore, higher *GCN1* and *GCN2* expression was present in cancer versus normal adjacent tissues in the TCGA and other patient cohorts (**Fig. 4I**; Supplementary Fig. S4D). In terms of association between expression and patient prognosis, there was a trend towards higher *GCN1* expression being associated with poorer prognosis, but *GCN2* expression was not predictive of prognosis in prostate cancer (Supplementary Fig. S4E). In summary, GCN1 and GCN2 are expressed across different tumor types and although highly expressed in prostate cancer, they do not predict patient prognosis.

MIRO2 regulates GCN2 signaling

Given that loss of function of GCN1, GCN2, or MIRO2 impaired tumor cell growth; we next asked whether MIRO2 may modulate GCN1′s function as an activator of GCN2. GCN1 helps GCN2 sense deacylated tRNA that accumulates upon amino acid scarcity, leading to auto-phosphorylation of GCN2, and downstream phosphorylation of the eukaryotic translation initiation factor 2α (eIF2α, **Fig. 5A**). Phosphorylated eIF2α shuts off global protein translation, while concomitantly inducing selective translation of the transcriptional activator 4 (ATF4; refs. 29, 30). Due to the robust interaction between MIRO2 and GCN1, we hypothesized that MIRO2 regulates GCN2 signaling. When GCN2 activation was induced by AAS we found that MIRO2 depletion impaired p-GCN2, p-eIF2α, and ATF4 levels in prostate cancer (**Fig. 5B** and C; Supplementary Fig. S5A and S5B). On the contrary, MIRO1 depletion did not affect the levels of p-GCN2, p-eIF2α, and ATF4 in response to AAS (Supplementary Fig. S5C and S5D). Thus, we have demonstrated for the first time that MIRO2 is a novel regulator of GCN2 signaling in prostate cancer cells.

Because the MIRO2-GCN1 interaction was undetectable in benign prostate epithelial cell lines, we next evaluated whether GCN2 could be differentially activated in prostate cancer cells. To this end, we compared the effects of AAS in HPrEC or immortalized by telomerase bypass or viral transformation (EP156T and RWPE1 respectively). Indeed, we found that benign cell lines did not activate GCN2 upon AAS (**Fig. 5D**). This suggests that the MIRO2-GCN1-GCN2 signaling cascade is selectively activated in cancer cells over normal cells.

To test the relevance of this pathway *in vivo*, we examined the activation status of GCN2 in xenografts from control or MIRO2-depleted cancer cell lines. We used a p-GCN2 antibody that was blocked by phospho-T899-GCN2 peptide binding prior to IHC (Supplementary Fig. S5E and S5F). Phosphorylated-GCN2 levels were lower in MIRO2-depleted xenografts compared with control (PC3, **Fig. 5E** and **F**; DU145, Supplementary Fig. S5G and S5H). On the contrary, total levels of GCN2 did not change between control and MIRO2-depleted xenografts. Furthermore, p-GCN2 and MIRO2 levels were positively correlated (PC3, **Fig. 5G**; DU145, Supplementary Fig. S5I). Overall, GCN2 is activated in prostate cancer xenografts in a MIRO2-dependent manner.

MIRO2 controls the levels and activity of ATF4 in prostate cancer

Since translation of ATF4 is a key step downstream of the activation of GCN2, we next evaluated a potential link between MIRO2 and ATF4. Interestingly, MIRO2 was required for maximal ATF4 induction in response to nutrient starvation both in AR-independent and androgen-sensitive cell lines (**Fig. 6A** and **B**). We next examined whether GCN1 and GCN2 are the main regulators of ATF4 levels in these conditions. Knockdown of GCN1 or GCN2 reduced ATF4 levels in response to AAS in all cell lines except for DU145 (Supplementary Fig. S6A and S6B). Interestingly, MIRO2 or GCN1 depletion partially

Figure 4.

GCN1/2 regulation of prostate cancer cell growth. **A,** Dependency scores predicting the likelihood of GCN1 or GCN2 genes being essential on the prostate cancer cell lines indicated. Scores were retrieved from the DepMap portal (Broad Institute) from genome-wide RNAi or CRISPR based screens for vulnerabilities of cancer cells. **B** and **C**, Stable knockdown of GCN1 or GCN2 was achieved by either shRNA in PC3 and DU145 cells, or siRNA in C4–2 and 22rv1 cells. **B,** Representative blots showing the efficiency of knockdown. **C,** Anchorage-independent growth in soft agar at 14 days postplating. Colony number per well was quantitated, relativized to control, and represented as mean ± SEM ($n = 3$). ***, $P < 0.001$ by ANOVA and Dunnett posttest for pairwise comparisons to control group. Control sh/si; G1a/b, GCN1-targeting shRNAs (sequence a and b); G2a/b, GCN2-targeting shRNAs (sequence a and b); G1, GCN1 siRNA pool; G2, GCN2 siRNA pool. **D,** MIRO2 mutations observed in patients with prostate cancer. PC, prostate cancer. **E,** PC3 cells expressing stable MIRO2 shRNA were transfected with the indicated FLAG-tagged MIRO2 constructs, subject to Flag-IP and analyzed by Western blot for co-IP of GCN1. A representative blot from $n = 3$ experiments is shown. **F,** Levels of immunoprecipitated GCN1 were normalized to MIRO2 immunoprecipitated levels, relativized to MIRO2 WT, and represented as mean ± SEM ($n = 3$). NS, not significant ($P > 0{,}05$); *, $P < 0.05$ by ANOVA and Dunnett posttest for pairwise comparisons to control group. **G,** PC3 cells expressing stable MIRO2 shRNA were transfected with the indicated FLAG-tagged MIRO2 constructs and analyzed for anchorage-independent growth. PC3 control cells expressing control sh were transfected with empty vector and used as control. Colony number per well was quantitated, relativized to control and represented as mean ± SEM ($n = 3$). ***, $P < 0.001$ by ANOVA and Dunnett posttest for pairwise comparisons to control group. **H,** The TCGA database was interrogated for *GCN1/2* mRNA expression across tumor types. **I,** Relative expression of *GCN1/2* mRNA in cancer versus normal adjacent tissues on the prostate TCGA PanCancer study. C, control; TM, transmembrane domain.

reduced ATF4 levels, but GCN2 depletion completely abolished basal and AAS-stimulated ATF4 levels (Supplementary Fig. S6A and S6B). Furthermore, ATF4 levels were positively correlated to p-GCN2 levels in prostate cancer xenografts (Supplementary Fig. S6C), reinforcing a role of GCN2 in maintaining ATF4 levels *in vitro* and *in vivo*.

To address if MIRO2-dependent expression of ATF4 results in higher transcriptional activity of ATF4, an ATF4 luciferase reporter was used (**Fig. 6C**). Indeed, induction of ATF4 transcriptional activity in response to AAS was dependent on MIRO2 expression (**Fig. 6C**). Although 2D cell growth was impaired by AAS, with MIRO2 depleted cells growing slower than control cells, the differences were not statistically significant (Supplementary Fig. S6D). Importantly, ATF4 transcriptional activity was positively regulated by MIRO2 both in amino acid–replete and in AAS conditions (**Fig. 6C**; Supplementary Fig. S6E). Overall, MIRO2 controls the levels and activity of ATF4 in AR-independent and androgen-sensitive prostate cancer cell lines.

ATF4 controls the expression of a wide range of adaptive genes that allows cancer cells to adapt to excessive proliferation and demanding tumor microenvironment conditions (30). To determine whether ATF4 is required for prostate cancer cell growth, we mined the Cancer Dependency Map. Depletion of ATF4 via RNAi or CRISPR/Cas9 gene editing in a panel of prostate cancer cell lines reduced cell growth (score < 0) in all cell lines tested (**Fig. 6D**). As MIRO2 controlled ATF4 levels in prostate cancer, we next sought to assess whether lower levels of ATF4 in MIRO2-depleted cells could explain reduced prostate cancer cell growth. To this extent, we expressed human ATF4 cDNA in control or MIRO2-depleted cells. We found that transient ATF4 expression rescued anchorage-independent growth of MIRO2-depleted cells to control levels in the four prostate cancer cell lines tested (**Fig. 6E**). Overall, ATF4 is the main mediator of MIRO2 in regulating prostate cancer cell growth.

To test the relevance of ATF4 *in vivo*, we examined the levels of ATF4 in xenografts from control or MIRO2-depleted cancer cell lines. ATF4 levels were lower in MIRO2-depleted xenografts compared with control (PC3, **Fig. 6F** and **G**; DU145, Supplementary Fig. S6F and S6G). Furthermore, ATF4 levels were positively correlated with both MIRO2 (PC3, **Fig. 6H**; DU145, Supplementary Fig. S6H) and p-GCN2 levels (PC3, Supplementary Fig. S6C). Overall, ATF4 levels are dependent on MIRO2 expression in prostate cancer xenografts.

GCN2 is activated in hypoxic areas *in vivo*

In addition to amino acid depletion, GCN2 is activated by redox status and actin dynamics cues in cells (29, 30). Common tumor microenvironment conditions, such as glucose starvation and hypoxia, could lead to changes in metabolism and oxidation of amino acid as alternative fuels. Furthermore, rapidly growing tumors experience a high rate of protein synthesis, accompanied by amino acid shortage. We hypothesize that these diverse intratumoral conditions may lead to amino acid shortage and activation of p-GCN2.

To begin understanding how GCN2 may be regulated in an *in vivo* context, we explored a potential link between hypoxia or glucose starvation and p-GCN2 levels. Xenografts from PC3 cells expressing endogenous MIRO2 levels showed areas of relative hypoxia, based on accumulation of the hypoxia-inducible factor 1α (HIF1α, **Fig. 7A** and **B**). The areas of higher hypoxia were associated with increased levels of p-AMPK, a marker of glucose starvation (**Fig. 7A** and **B**), consistent with areas of poor perfusion/vascularization. While total GCN2 levels did not change, p-GCN2 levels were higher in areas of hypoxia (**Fig. 7A** and **B**) and the intensity of p-GCN2 and HIF1α were positively correlated (**Fig. 7C**). Interestingly, we found that MIRO2 levels were elevated in hypoxic areas as well (**Fig. 7A** and **B**). In order to examine the relevance of these findings in clinical datasets, we analyzed the TCGA prostate adenocarcinoma PanCancer dataset for association between *MIRO2* and hypoxia. We found a positive correlation between the Buffa hypoxia scores (37), based on coexpression of common hypoxia gene signatures with high prognostic value in multiple cancers, and *MIRO2* mRNA (**Fig. 7D**). In summary, we found an association between hypoxia and higher levels of p-GCN2 and MIRO2 in prostate cancer xenografts and patient datasets.

Discussion

In this study, we have shown that *MIRO2* mRNA expression is upregulated in prostate cancer and that higher levels of *MIRO2* correlate with poor patient survival in prostate cancer cohorts. This is in agreement with previous studies where *MIRO2* was overexpressed in cancer compared with benign tissues across disparate tumor types (13). Interestingly, the closely related *MIRO1* was downregulated at the mRNA level, and did not correlate with patient survival. This is the first evidence that *MIRO1* and *MIRO2* are oppositely regulated in prostate cancer. Furthermore, we found that prostate cancer that recurred or progressed expressed higher levels of *MIRO2*, suggesting that *MIRO2* is important for prostate cancer tumor progression.

Our studies show that MIRO2 is required for growth of prostate cancer in cell lines representing AR-independent and androgen-sensitive disease. Furthermore, MIRO2 depletion impaired tumor growth *in vivo*, which was associated with *in situ* decreased proliferation of tumor cells. Recently, MIRO2 was linked to regulation of cancer cell motility and metastasis (16). In these studies, Myc overexpression led to reprogramming of the mitochondrial network to fuel focal adhesion dynamics and motility. In contrast, we found that under basal conditions of endogenous expression of Myc, prostate cancer cells did not show alterations in gross mitochondrial distribution inside cells. One possibility is that Myc overexpression favors higher expression of MIRO1, MIRO2, and other mitochondrial trafficking proteins, thus enabling enhanced mitochondrial trafficking. Interestingly, our data indicates that MIRO1 is not required for regulating prostate cancer cell growth. To date, this is one of the first observations where MIRO1 and MIRO2 show divergent functions in mammalian cells.

Our proteomics approach identified novel protein binders of MIRO2 in prostate cancer cells. Previously, known interactors of MIRO2 in neurons or fibroblasts included TRAK proteins that link MIRO2 to microtubules (38, 39). In our studies, MIRO2 did not coprecipitate with TRAK, nor did it alter mitochondrial distribution within cancer cells. Other protein binders of MIRO2 in nontumorigenic cells include the E3 ubiquitin ligase Parkinson Protein 2 (PARK2) and the kinesin-like protein motor Centromere Protein F (CENPF; refs. 26, 40). Of note, association to PARK2 occurs exclusively under severe stress induced by treatment with mitochondrial uncouplers (26), and association to CENPF is exclusively detected in *M* phase of the cell cycle (40). The fact that these previously known MIRO binding partners were not present in our IP screen may be because our studies were carried out in prostate cancer cells that were not stressed or arrested on *M* phase of the cell cycle. Alternatively, cancer cells may have a largely nonoverlapping interactome with normal cells. This idea warrants further exploration, as there are no other available proteomic studies identifying MIRO2 binding partners in normal *versus* cancer cells.

In this study, we focused our efforts in characterizing the function of GCN1, a previously unknown protein binder of MIRO2. Our data shows that GCN1 is needed for anchorage-dependent and

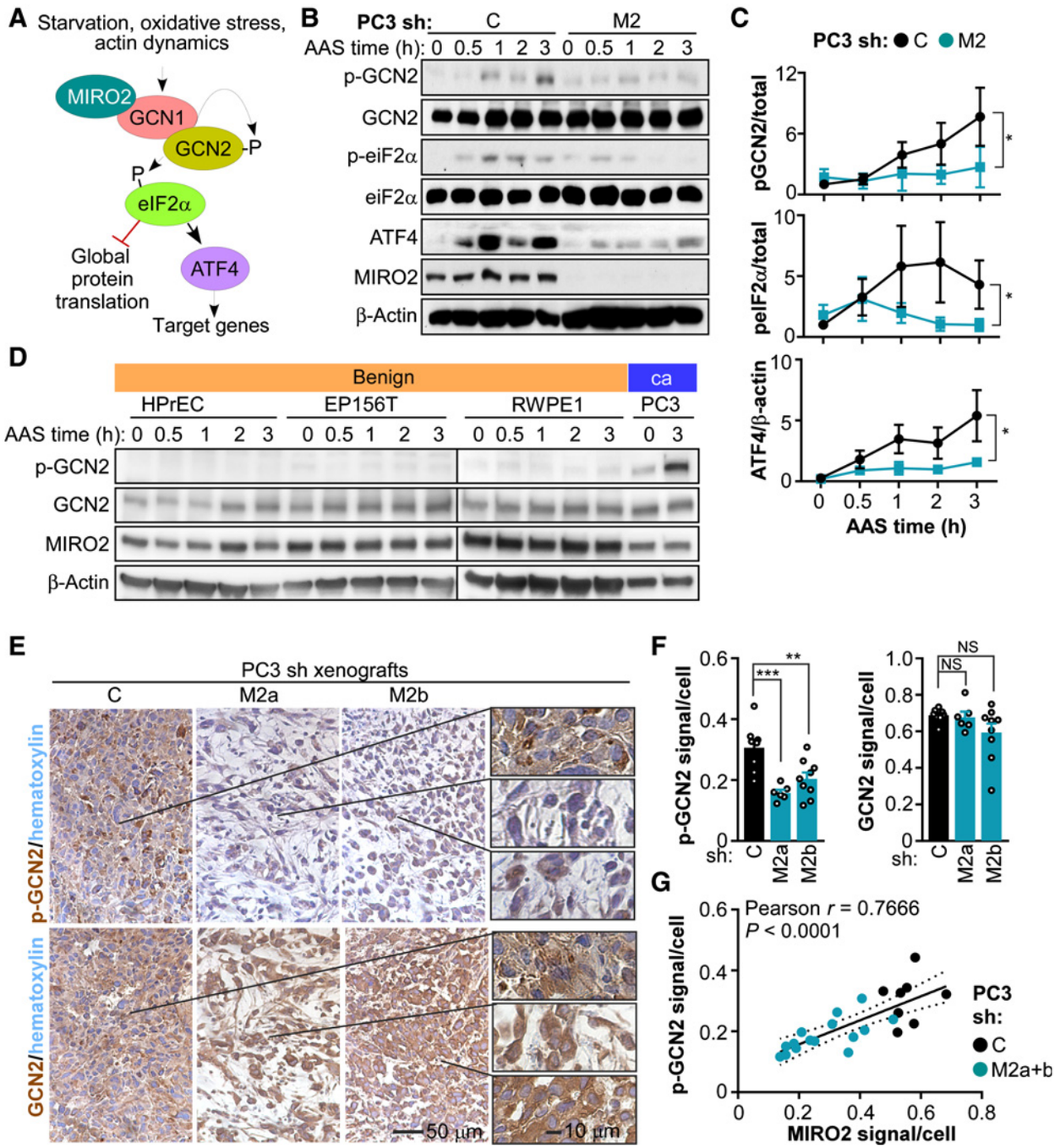

Figure 5.

MIRO2 regulates GCN2 signaling. **A,** Canonical function of GCN1 as a coactivator of GCN2 signaling by amino acid/glucose starvation, oxidative stress, and actin dynamics. **B,** PC3 cells expressing control sh or MIRO2-sh were incubated in AAS conditions for 0 to 3 hours and subjected to Western blot. **C,** Densitometry analysis of the blots from (**B**). Data is expressed as mean ± SEM. ($n = 3$). *, $P < 0.05$ by one-way ANOVA and Tukey posttest. **D,** HPrEC, immortalized prostate epithelial (EP156T and RWPE1), or PC3 cells were incubated in full medium or AAS conditions for 0 to 3 hours and subjected to Western blot. A representative gel is shown ($n = 3$). **E,** Xenografts from PC3 cells expressing control or MIRO2-sh were subject to IHC. Representative images at 10X magnification. **F,** 3,3′-Diaminobenzidine (DAB) signal intensity per field was quantitated, normalized to the number of nuclei in the same field and represented as mean ± SEM. ($n = 3$). ***, $P < 0.0001$ by one-way ANOVA and Dunnett posttest. NS, not significant. **G,** Correlation between MIRO2 and p-GCN2 signal/cell in tumors from (**E**). C, control; Csh, control sh; M2sh, MIRO2-sh.

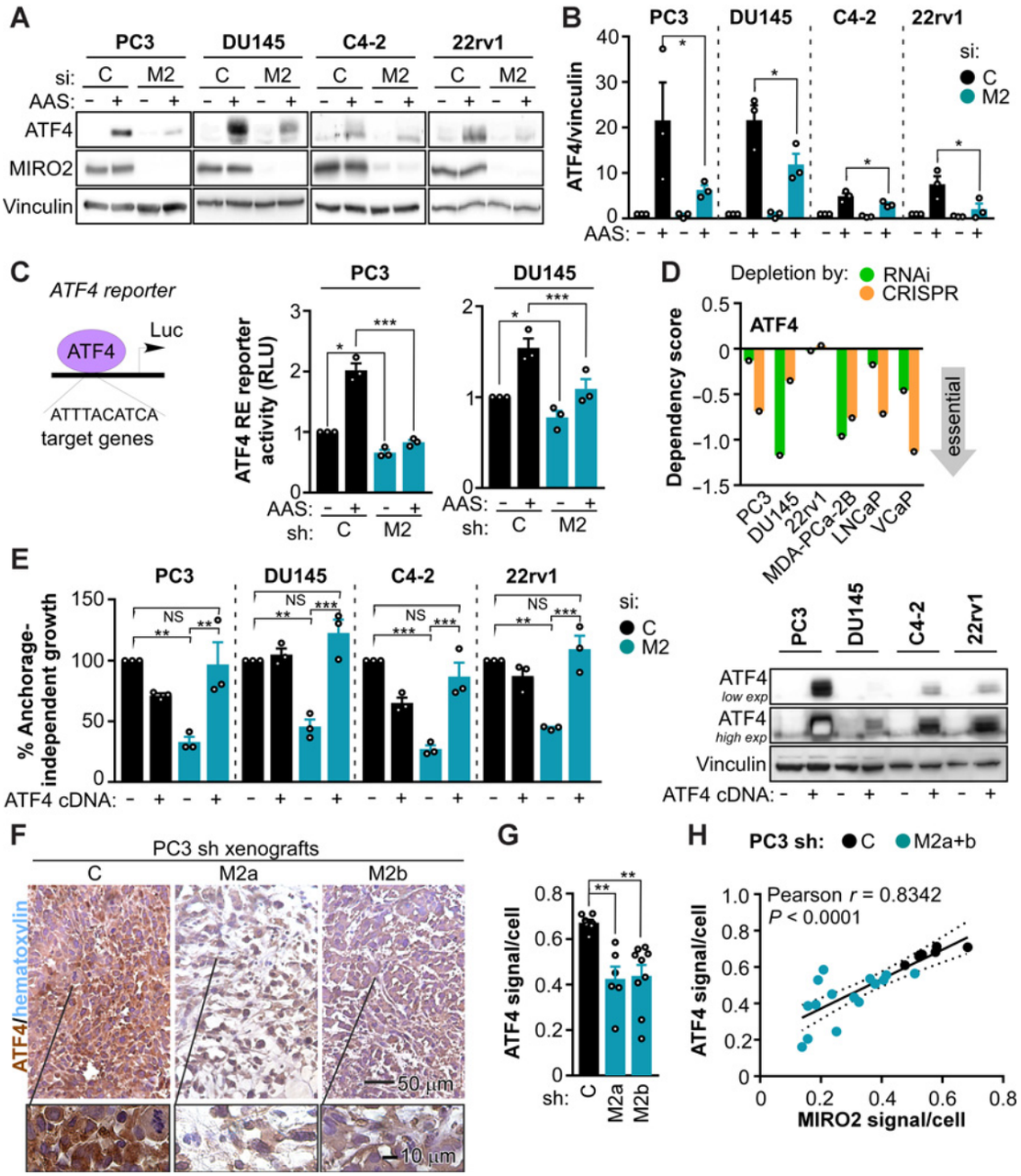

Figure 6.

MIRO2 regulates ATF4 in prostate cancer. **A,** Cells were transfected with control or MIRO2-targeting RNAi, and 96 hours later were treated for 3 hours in full (AAS^-) or amino acid–depleted medium (AAS^+). Representative Western blots ($n = 3$) are shown. **B,** Densitometry analysis of the blots from (A). Data is relativized to control cells in full medium and expressed as mean ± SEM. ($n = 3$). *, $P < 0.05$ by one-way ANOVA and Tukey posttest for multiple comparisons. **C,** The indicated cell lines expressing control or MIRO2-targeting RNAi were cotransfected with ATF4-RE-Firefly luciferase and constitutive TK-Renilla reporter constructs and treated for 24 hours in full or AAS depleted medium. Left, ATF4 reporter scheme. Right, ATF4 RE reporter activity was normalized to TK-Renilla and represented as mean ± SEM ($n = 3$). *, $P < 0.01$; ***, $P < 0.0001$ by ANOVA and Tukey posttest for multiple comparisons. **D,** Dependency scores predicting the likelihood of ATF4 being an essential gene on the prostate cancer cell lines indicated. Scores were retrieved from the DepMap portal (Broad Institute) from genome-wide RNAi or CRISPR-based screens for vulnerabilities of cancer cells. **E,** Prostate cancer cells were sequentially transfected with control or MIRO2-targeting siRNA followed by with empty vector ($^-$) or ATF4 cDNA ($^+$) and assayed for anchorage-independent growth. Left, data are relativized to control with empty vector and represented as mean ± SEM ($n = 3$). *, $P < 0.01$ by ANOVA and Dunnett posttest for multiple comparisons to the control group. Right, representative blots ($n = 3$) showing levels of expression of ATF4 in M2 KD cells. **F** to **H**, Xenografts from PC3 cells expressing control or MIRO2-sh were subject to IHC. **F,** Representative images at 40X magnification (inset taken at 100X magnification). **G,** DAB signal intensity per field was quantitated, normalized to the number of nuclei in the same field, and represented as mean ± S.E.M. ($n = 3$). **, $P < 0.01$ by one-way ANOVA and Dunnett posttest. **H,** Correlation between MIRO2 and ATF4 signal/cell in tumors from (**F**). C, control; MIRO2, M2; Csh, control sh; esp, exposure; M2sh, MIRO2-sh; NS, not significant.

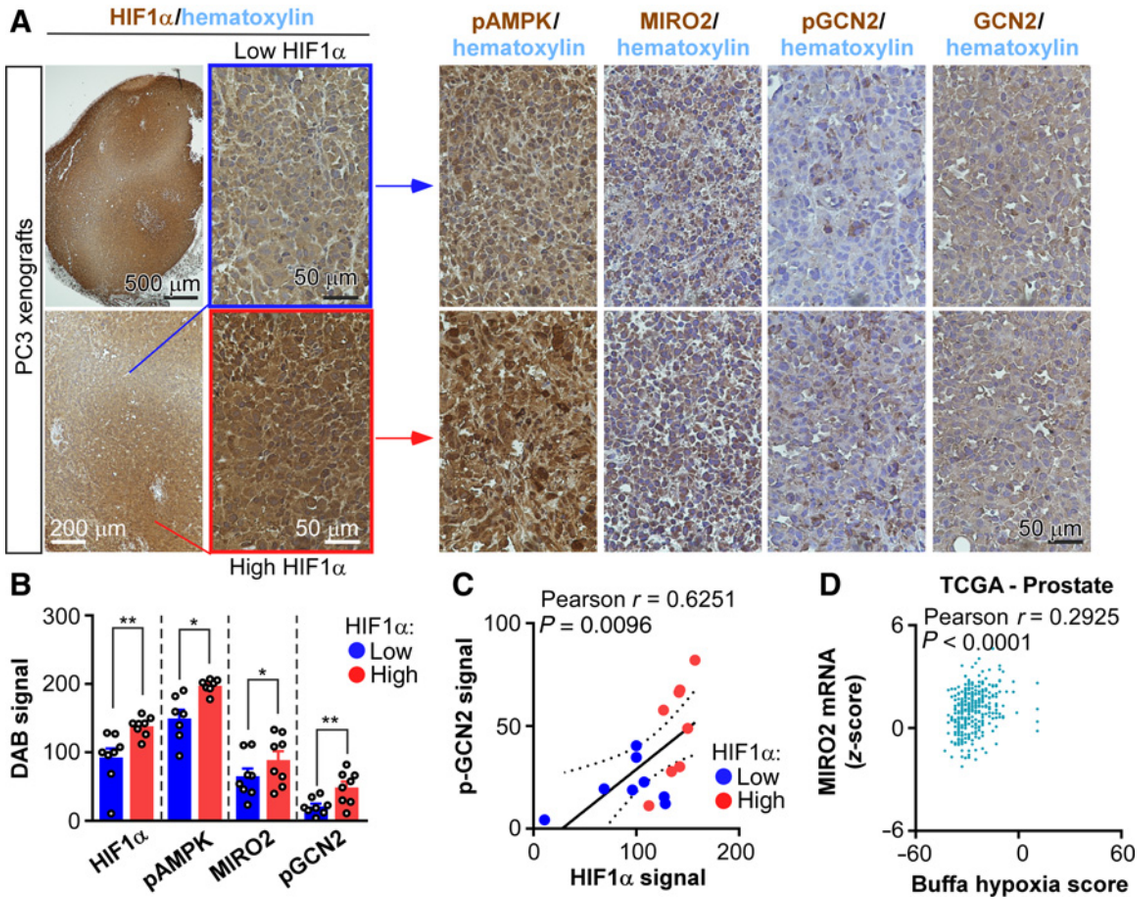

Figure 7.

Regulation of p-GCN2 *in vivo*. **A** to **C**, Xenografts from PC3 cells expressing endogenous levels of MIRO2 were subject to IHC ($n = 8$). **A,** Left, representative images from a single xenograft tumor at 4 to 40X magnification showing areas of relative low versus high HIF1α staining. Right, areas of low or high HIF1α staining were analyzed for staining of the indicated proteins. **B,** DAB signal intensity per field was quantitated, normalized to the number of nuclei in the same field and represented as mean ± SEM. ($n = 3$). *, $P < 0.05$; **, $P < 0.01$ by one-way ANOVA and Dunnett posttest. **C,** Correlation between p-GCN2 and HIF1α signal in tumors from (**B**). **D,** Correlation between *MIRO2* expression and Buffa hypoxia score on the TCGA prostate adenocarcinoma database ($n = 333$).

-independent growth of AR-independent and androgen-sensitive prostate cancer cells. Furthermore, GCN1 was a common essential gene in a large panel of pan-cancer cell lines. Altogether, these are the first data implicating GCN1 in controlling cancer cell biology. Interestingly, GCN1 was also overexpressed in prostate cancer compared with benign tissue and the interaction of MIRO2-GCN1 was increased in prostate cancer *versus* immortalized prostate epithelial cells. Thus, our data suggests that targeting the MIRO2-GCN1 axis may selectively affect tumors while minimizing side effects on normal tissues.

The canonical function of GCN1 is to activate the kinase GCN2 in response to AAS, accumulation of globular actin, or oxidative stress (29). However, recent evidence points to GCN2-independent effects of GCN1 in the control of inflammatory and tissue remodeling responses (41). In our studies, we found that MIRO2 was required for activation of GCN2 signaling in prostate cancer cells. In prostate cancer xenograft tumors, MIRO2 levels were correlated with activation of GCN2 (p-GCN2), reinforcing that MIRO2 is a novel regulator of GCN2 signaling in prostate cancer. Furthermore, GCN1 and GCN2 were required for anchorage-dependent and -independent growth of prostate cancer cells. Thus, GCN1′s canonical function as an activator of GCN2 is important for prostate cancer cell growth.

As the MIRO2-GCN1 complex has not been structurally characterized yet, we lack the insight to generate tools that will selectively disrupt the MIRO2-GCN1 interaction without affecting binding to other binders of MIRO2. Thus, we cannot assign the relative contribution of the MIRO2-GCN1 interaction to supporting prostate cancer cell growth. However, we gained some insight in terms of regulation of the MIRO2-GCN1 interaction *in vivo*. We characterized the function of six MIRO2 mutations observed in prostate cancer patient cohorts and found that mutation of F159 L on MIRO2 increased GCN1 binding. A recent study described a conserved surface of the *N*-terminal GTPase of MIRO2 termed the "SELFYY" motif, which spans from aa156 to 161 (42). It has been proposed that the SELFYY motif (which contains F159) may be involved in dimerization and interaction with binding partners (42), thus we hypothesize that mutation to F159 L increases binding to GCN1 through increased dimerization of mutant MIRO2. On the other hand, mutation of MIRO2 at S277R led to decreased GCN1 binding. We speculate that the S277R mutation, which is located within one of the EF-hands, may impede calcium-dependent conformation changes of the EF-hand that are required for maximal binding to GCN1. A limitation of our studies is that we do not know whether these mutations regulate GCN1 binding specifically or

whether they affect binding of MIRO2 to other binders as well. In the future, additional studies will be needed to examine the potential effect of these MIRO2 mutations in prostate cancer cell growth *in vitro* and *in vivo*. In sum, we observed that prostate cancer cell growth was dependent on MIRO2 and GCN1.

In agreement with previous studies in fibrosarcoma (32), GCN2 was activated in prostate cancer xenograft tumors. Such activation of GCN2 in tumors may result from: (i) a challenging microenvironment depleted of oxygen and nutrients, or (ii) tumor metabolic rewiring to redirect available nutrients into anabolic pathways to support tumor proliferation and biomass expansion. In our studies, we found an association between higher hypoxia and glucose starvation with higher levels of MIRO2 and increased p-GCN2 in prostate cancer xenografts. Furthermore, *MIRO2* mRNA levels were positively correlated with the hypoxic score of prostate cancer tumors in the TCGA prostate adenocarcinoma database. Overall, these data suggest that hypoxia may drive activation of the MIRO2/GCN1/GCN2 pathway *in vivo*.

An open question that stems from our studies is what are the upstream signals that trigger MIRO2-dependent GCN1/2 activation in prostate cancer cells. As MIRO2 is a mitochondrial protein located in the outer mitochondrial membrane, it may be ideally located to sense and transduce mitochondrial fitness signals back to the nucleus by engaging GCN1/2-dependent retrograde signaling. In support of this idea, studies in worms and nontransformed mammalian cells have shown that reactive oxygen species (ROS) or amino acid depletion engage GCN2 retrograde signaling (35, 36). We do not know whether this mechanism is at play in prostate cancer cells, or how local pools of mitochondrially produced ROS and amino acid levels engage MIRO2-GCN1. However, the fact that the MIRO2-GCN1 interaction, and MIRO2-dependent activation of GCN2 selectively occur in cancer cells suggests that transformed cells benefit from having a pool of GCN1/2 locally activated at the mitochondrial surface.

In terms of the downstream mechanisms that mediate tumor cell growth downstream of MIRO2, we show that ATF4 mediates MIRO2 effects in prostate cancer cell growth. Interestingly, MIRO2 controls ATF4 transcriptional activity both in amino acid–replete and in amino acid– depleted conditions. In prostate cancer cells, ATF4 is essential for cell growth, and ATF4 expression rescues cell growth of MIRO2-depleted cells. Furthermore, ATF4 levels in prostate cancer xenografts are correlated to MIRO2 expression. Overall, this indicates that MIRO2 positively regulates ATF4 levels and that contributes to prostate cancer cell growth. However, other potential mechanisms, including global protein translation control downstream of GCN2 may be at play.

Our studies show that induction of ATF4 levels by AAS is dependent on GCN1 and GCN2 in three of the four prostate cancer cell lines tested (PC3, C4–2, and 22rv1), but seems independent of both GCN1 and GCN2 in DU145 cells. While we do not know the mechanisms behind this divergent response, we note that all four cell lines were dependent on MIRO2 for induction of ATF4 under AAS. In this context, we cannot rule out a potential role of MIRO2 in controlling additional stress sensing kinases that converge on eIF2α/ATF4, including the ER stress sensor EIF2AK3 (43, 44). Because MIRO2 has been linked to ER-mitochondrial signaling in normal cells (24), the possibility that MIRO2 is a broad regulator of kinases converging on eIF2α/ATF4 will need further exploration.

In summary, we identified a novel signaling pathway centered on MIRO2 that is required for growth of prostate cancer cells *in vitro* and *in vivo*. MIRO2 relies on activation of GCN1/2 signaling and ATF4 induction to support prostate cancer cell growth. *MIRO2* and *GCN1* are both overexpressed in prostate cancer patient cohorts, and the MIRO2-GCN1 interaction occurs selectively in prostate cancer cells. We therefore propose that targeting the MIRO2-GCN1 axis may be a valuable strategy to halt prostate cancer growth. We speculate that targeting this pathway in metastatic castrate-resistant prostate cancer (mCRPC) or AR-independent metastatic prostate cancer, where AR interventions are not effective (3–7), may be a good therapeutic strategy.

Authors' Disclosures

M. Furnish reports grants from NIH T32; and grants from Boettcher Foundation during the conduct of the study. D.P. Boulton reports grants from NIH during the conduct of the study. S.D. Cramer reports grants from NIH during the conduct of the study. M.C. Caino reports grants from Boettcher Foundation, NIH/National Institute of General Medical Sciences (NIGMS), Department of Defense, Cancer League of Colorado; and grants from American Cancer Society (ACS) during the conduct of the study. No disclosures were reported by the other authors.

Authors' Contributions

M. Furnish: Formal analysis, investigation, methodology, writing–review and editing. **D.P. Boulton:** Formal analysis, investigation, methodology, writing–original draft, writing–review and editing. **V. Genther:** Investigation, methodology, writing–review and editing. **D. Grofova:** Investigation. **M.L. Ellinwood:** Investigation. **L. Romero:** Resources, investigation. **M.S. Lucia:** Resources. **S.D. Cramer:** Resources, methodology, writing–review and editing. **M.C. Caino:** Conceptualization, formal analysis, supervision, funding acquisition, validation, investigation, methodology, writing–original draft, project administration, writing–review and editing.

Acknowledgments

The authors acknowledge Monika Dzieciatkowska for proteomics sample preparation and analysis, and the Histology Core for histology services, and Dr. Andrew Thorburn for critically reading the manuscript. This work was supported by the ACS IRG-16-184-56 (to M.C. Caino); Boettcher Foundation AWD-193249 (to M.C. Caino); Office of the Assistant Secretary of Defense for Health Affairs through the Prostate Cancer Research Program under award no. W81XWH-21-1-0408 (to M.C. Caino and V. Genther); NIH R35 GM142774 (to M.C. Caino, D.P. Boulton, and D. Grofova); and T32 GM007635 (M. Furnish, D.P. Boulton); and The Cancer League of Colorado AWD-193451-JT (to M.L. Ellinwood). Cancer Center Support Grant (CSSG) P30 CA046934 to the University of Colorado Cancer Center provided support of Core Facilities utilized in this study. Opinions, interpretations, conclusions, and recommendations are those of the authors and are not necessarily endorsed by the any of the funders, including the Department of Defense.

The costs of publication of this article were defrayed in part by the payment of page charges. This article must therefore be hereby marked *advertisement* in accordance with 18 U.S.C. Section 1734 solely to indicate this fact.

Received May 20, 2021; revised November 19, 2021; accepted December 22, 2021; published first January 6, 2022.

References

1. Crawford ED, Heidenreich A, Lawrentschuk N, Tombal B, Pompeo ACL, Mendoza-Valdes A, et al. Androgen-targeted therapy in men with prostate cancer: evolving practice and future considerations. Prostate Cancer Prostatic Dis 2019;22:24–38.
2. Teo MY, Rathkopf DE, Kantoff P. Treatment of advanced prostate cancer. Annu Rev Med 2019;70:479–99.
3. Tsaur I, Heidegger I, Kretschmer A, Borgmann H, Gandaglia G, Briganti A, et al. Aggressive variants of prostate cancer - Are we ready to apply specific treatment right now? Cancer Treat Rev 2019;75:20–6.
4. Watson PA, Arora VK, Sawyers CL. Emerging mechanisms of resistance to androgen receptor inhibitors in prostate cancer. Nat Rev Cancer 2015;15:701–11.

5. Jonnalagadda B, Arockiasamy S, Krishnamoorthy S. Cellular growth factors as prospective therapeutic targets for combination therapy in androgen independent prostate cancer (AIPC). Life Sci 2020;259:118208.
6. Laudato S, Aparicio A, Giancotti FG. Clonal evolution and epithelial plasticity in the emergence of AR-independent prostate carcinoma. Trends Cancer 2019;5: 440–55.
7. Mollica V, Di Nunno V, Cimadamore A, Lopez-Beltran A, Cheng L, Santoni M, et al. Molecular mechanisms related to hormone inhibition resistance in prostate cancer. Cells 2019;8:43.
8. Zong WX, Rabinowitz JD, White E. Mitochondria and Cancer. Mol Cell 2016;61: 667–76.
9. Bader DA, Hartig SM, Putluri V, Foley C, Hamilton MP, Smith EA, et al. Mitochondrial pyruvate import is a metabolic vulnerability in androgen receptor-driven prostate cancer. Nat Metab 2019;1:70–85.
10. Caino MC, Altieri DC. Molecular pathways: mitochondrial reprogramming in tumor progression and therapy. Clin Cancer Res 2016;22:540–5.
11. Caino MC, Chae YC, Vaira V, Ferrero S, Nosotti M, Martin NM, et al. Metabolic stress regulates cytoskeletal dynamics and metastasis of cancer cells. J Clin Invest 2013;123:2907–20.
12. Weinberg SE, Chandel NS. Targeting mitochondria metabolism for cancer therapy. Nat Chem Biol 2015;11:9–15.
13. Caino MC, Seo JH, Aguinaldo A, Wait E, Bryant KG, Kossenkov AV, et al. Altieri DC. A neuronal network of mitochondrial dynamics regulates metastasis. Nat Commun 2016;7:13730.
14. Lopez-Domenech G, Covill-Cooke C, Ivankovic D, Halff EF, Sheehan DF, Norkett R, et al. Miro proteins coordinate microtubule- and actin-dependent mitochondrial transport and distribution. EMBO J 2018;37:321–36.
15. Caino MC, Ghosh JC, Chae YC, Vaira V, Rivadeneira DB, Faversani A, et al. PI3K therapy reprograms mitochondrial trafficking to fuel tumor cell invasion. Proc Natl Acad Sci U S A 2015;112:8638–43.
16. Agarwal E, Altman BJ, Ho Seo J, Bertolini I, Ghosh JC, Kaur A, et al. Myc regulation of a mitochondrial trafficking network mediates tumor cell invasion and metastasis. Mol Cell Biol 2019;39:e00109–19.
17. Barclay WW, Woodruff RD, Hall MC, Cramer SD. A system for studying epithelial-stromal interactions reveals distinct inductive abilities of stromal cells from benign prostatic hyperplasia and prostate cancer. Endocrinology 2005;146: 13–8.
18. Cerami E, Gao J, Dogrusoz U, Gross BE, Sumer SO, Aksoy BA, et al. The cBio cancer genomics portal: an open platform for exploring multidimensional cancer genomics data. Cancer Discov 2012;2:401–4.
19. Gao J, Aksoy BA, Dogrusoz U, Dresdner G, Gross B, Sumer SO, et al. Integrative analysis of complex cancer genomics and clinical profiles using the cBioPortal. Sci Signal 2013;6:pl1.
20. Devine MJ, Birsa N, Kittler JT. Miro sculpts mitochondrial dynamics in neuronal health and disease. Neurobiol Dis 2016;90:27–34.
21. Fransson S, Ruusala A, Aspenstrom P. The atypical Rho GTPases Miro-1 and Miro-2 have essential roles in mitochondrial trafficking. Biochem Biophys Res Commun 2006;344:500–10.
22. Wu TT, Sikes RA, Cui Q, Thalmann GN, Kao C, Murphy CF, et al. Establishing human prostate cancer cell xenografts in bone: induction of osteoblastic reaction by prostate-specific antigen-producing tumors in athymic and SCID/bg mice using LNCaP and lineage-derived metastatic sublines. Int J Cancer 1998;77:887–94.
23. Zhang T, Karsh LI, Nissenblatt MJ, Canfield SE. Androgen receptor splice variant, AR-V7, as a biomarker of resistance to androgen axis-targeted therapies in advanced prostate cancer. Clin Genitourin Cancer 2020;18:1–10.
24. Modi S, Lopez-Domenech G, Halff EF, Covill-Cooke C, Ivankovic D, Melandri D, et al. Miro clusters regulate ER-mitochondria contact sites and link cristae organization to the mitochondrial transport machinery. Nat Commun 2019;10:4399.
25. Saotome M, Safiulina D, Szabadkai G, Das S, Fransson A, Aspenstrom P, et al. Bidirectional Ca2+-dependent control of mitochondrial dynamics by the Miro GTPase. Proc Natl Acad Sci U S A 2008;105:20728–33.
26. Shlevkov E, Kramer T, Schapansky J, LaVoie MJ, Schwarz TL. Miro phosphorylation sites regulate Parkin recruitment and mitochondrial motility. Proc Natl Acad Sci U S A 2016;113:E6097–106.
27. Fransson A, Ruusala A, Aspenstrom P. Atypical Rho GTPases have roles in mitochondrial homeostasis and apoptosis. J Biol Chem 2003;278:6495–502.
28. Vigil D, Cherfils J, Rossman KL, Der CJ. Ras superfamily GEFs and GAPs: validated and tractable targets for cancer therapy? Nat Rev Cancer 2010;10: 842–57.
29. Castilho BA, Shanmugam R, Silva RC, Ramesh R, Himme BM, Sattlegger E. Keeping the eIF2 alpha kinase Gcn2 in check. Biochim Biophys Acta 2014;1843: 1948–68.
30. Wortel IMN, van der Meer LT, Kilberg MS, van Leeuwen FN. Surviving stress: Modulation of ATF4-mediated stress responses in normal and malignant cells. Trends Endocrinol Metab 2017;28:794–806.
31. Yamazaki H, Kasai S, Mimura J, Ye P, Inose-Maruyama A, Tanji K, et al. Ribosome binding protein GCN1 regulates the cell cycle and cell proliferation and is essential for the embryonic development of mice. PLoS Genet 2020;16: e1008693.
32. Ye J, Kumanova M, Hart LS, Sloane K, Zhang H, De Panis DN, et al. The GCN2-ATF4 pathway is critical for tumour cell survival and proliferation in response to nutrient deprivation. EMBO J 2010;29:2082–96.
33. Falletta P, Sanchez-Del-Campo L, Chauhan J, Effern M, Kenyon A, Kershaw CJ, et al. Translation reprogramming is an evolutionarily conserved driver of phenotypic plasticity and therapeutic resistance in melanoma. Genes Dev 2017;31:18–33.
34. Nakamura A, Nambu T, Ebara S, Hasegawa Y, Toyoshima K, Tsuchiya Y, et al. Inhibition of GCN2 sensitizes ASNS-low cancer cells to asparaginase by disrupting the amino acid response. Proc Natl Acad Sci U S A 2018;115:E7776–85.
35. Baker BM, Nargund AM, Sun T, Haynes CM. Protective coupling of mitochondrial function and protein synthesis via the eIF2alpha kinase GCN-2. PLoS Genet 2012;8:e1002760.
36. Mick E, Titov DV, Skinner OS, Sharma R, Jourdain AA, Mootha VK. Distinct mitochondrial defects trigger the integrated stress response depending on the metabolic state of the cell. Elife 2020;9:e49178.
37. Buffa FM, Harris AL, West CM, Miller CJ. Large meta-analysis of multiple cancers reveals a common, compact and highly prognostic hypoxia metagene. Br J Cancer 2010;102:428–35.
38. Glater EE, Megeath LJ, Stowers RS, Schwarz TL. Axonal transport of mitochondria requires milton to recruit kinesin heavy chain and is light chain independent. J Cell Biol 2006;173:545–57.
39. MacAskill AF, Kittler JT. Control of mitochondrial transport and localization in neurons. Trends Cell Biol 2010;20:102–12.
40. Kanfer G, Courtheoux T, Peterka M, Meier S, Soste M, Melnik A, et al. Mitotic redistribution of the mitochondrial network by Miro and Cenp-F. Nat Commun 2015;6:8015.
41. Kim Y, Sundrud MS, Zhou C, Edenius M, Zocco D, Powers K, et al. Aminoacyl-tRNA synthetase inhibition activates a pathway that branches from the canonical amino acid response in mammalian cells. Proc Natl Acad Sci U S A 2020;117: 8900–11.
42. Smith KP, Focia PJ, Chakravarthy S, Landahl EC, Klosowiak JL, Rice SE, et al. Insight into human Miro1/2 domain organization based on the structure of its N-terminal GTPase. J Struct Biol 2020;212:107656.
43. Hamanaka RB, Bennett BS, Cullinan SB, Diehl JA. PERK and GCN2 contribute to eIF2alpha phosphorylation and cell cycle arrest after activation of the unfolded protein response pathway. Mol Biol Cell 2005;16:5493–501.
44. Harding HP, Zhang Y, Zeng H, Novoa I, Lu PD, Calfon M, et al. An integrated stress response regulates amino acid metabolism and resistance to oxidative stress. Mol Cell 2003;11:619–33.